

Electron dynamics of active mode-locking terahertz quantum cascade laser

Qiushi Hou(侯秋实)[1, 2], Chang Wang(王长)[1, 2, †], and Juncheng Cao(曹俊诚)[1, 2, ‡]

Citation: Chin. Phys. B, 2020, 29 (**12**): 127302. DOI: 10.1088/1674-1056/abc0da
Journal homepage: http://cpb.iphy.ac.cn; http://iopscience.iop.org/cpb

What follows is a list of articles you may be interested in

Electron dynamics of active mode-locking terahertz quantum cascade laser

Qiushi Hou(侯秋实)[1, 2], Chang Wang(王长)[1, 2, †], and Juncheng Cao(曹俊诚)[1, 2, ‡]
Chin. Phys. B, 2020, 29 (**12**): 127302. DOI: 10.1088/1674-1056/abc0da

Seeing Dirac electrons and heavy fermions in new boron nitride monolayers

Yu-Jiao Kang(康玉娇), Yuan-Ping Chen(陈元平), Jia-Ren Yuan(袁加仁), Xiao-Hong Yan(颜晓红), Yue-E Xie(谢月娥)
Chin. Phys. B, 2020, 29 (**5**): 057303. DOI: 10.1088/1674-1056/ab7e9e

Hydrodynamic simulation of chaotic dynamics in InGaAs oscillator in terahertz region

Wei Feng(冯伟)
Chin. Phys. B, 2020, 29 (**4**): 047302. DOI: 10.1088/1674-1056/ab696f

Quantum spin Hall insulators in chemically functionalized As (110) and Sb (110) films

Xiahong Wang(王夏烘), Ping Li(李平), Zhao Ran(冉召), Weidong Luo(罗卫东)
Chin. Phys. B, 2018, 27 (**8**): 087305. DOI: 10.1088/1674-1056/27/8/087305

Dynamic control of the terahertz rainbow trapping effect based on a silicon-filled graded grating

Shu-Lin Wang(王书林), Lan Ding(丁岚), Wen Xu(徐文)
Chin. Phys. B, 2017, 26 (**1**): 017301. DOI: 10.1088/1674-1056/26/1/017301

Electron dynamics of active mode-locking terahertz quantum cascade laser*

Qiushi Hou(侯秋实)[1,2], Chang Wang(王长)[1,2,†], and Juncheng Cao(曹俊诚)[1,2,‡]

[1] *Key Laboratory of Terahertz Solid-State Technology, Shanghai Institute of Microsystem and Information Technology, Chinese Academy of Sciences, Shanghai* 200050, *China*

[2] *Center of Materials Science and Optoelectronics Engineering, University of Chinese Academy of Sciences, Beijing* 100049, *China*

(Received 6 July 2020; revised manuscript received 30 September 2020; accepted manuscript online 14 October 2020)

The pulse generation from active mode-locking terahertz quantum cascade laser is studied by Maxwell–Bloch equations. It is shown that longer dephasing time will lead to multiple pulses generation from the laser. The dependence of output field on modulation length and radio-frequency parameters is obtained. In order to achieve short pulse generation, the DC bias should close to threshold value and modulation length should be shorter than 0.256 mm. The output pulse is unstable and the envelope shows many oscillations in the presence of spatial hole burning, resulting destabilization of mode-locking.

Keywords: terahertz (THz), quantum cascade lasers (QCLs), mode-locking, spatial hole burning (SHB)

PACS: 73.43.Cd, 78.30.Fs, 42.60.Fc **DOI:** 10.1088/1674-1056/abc0da

1. Introduction

Quantum cascade lasers (QCLs) based on electronic intersubband transitions in the conduction band of multilayered heterostructures are unipolar semiconductor lasers.[1] The major advantage of QCLs is spectral flexibility, the output frequency of the laser is dictated by the active region design.[2] In recent years, the widespread use of stable mode-locking lasers has promoted the development of chemistry, physics, and biology.[3–6] QCL provids a good candidate for realizing mode-locking technology. Since the first terahertz (THz) QCL invented in 2002, the generation of ultra-short pulses using THz QCLs has been developed with different approaches. The main purpose is to realize compact, electrically-pumped THz pulsed source, to study the dynamic characteristics of solid-state system by ultrafast spectroscopy, or to replace the THz time domain spectral system in practical applications.[7] The approach based on active mode-locking through radio-frequency (RF) modulation is the simplest solution to realize ultra-short pulse generation.

Active mode-locking of QCLs was reported by Paiella *et al.*[8] in 2000, the evidence of mode-locking is obtained from the measured optical spectral and the power spectral of the photocurrent. Wang *et al.*[9] studied mode-locking pulses generation in mid-infrared QCLs. The train of short pulses was generated by actively modulating the current. The pulse duration was characterized using a second-order interferometric autocorrelation technique based on a nonlinear quantum well infrared photodetector. Gkortsas *et al.*[10] have studied the impact of upper state lifetime limits and spatial hole burning (SHB) on achieving stable short pulse generation from actively mode-locking QCLs by numerical simulations. The effect of SHB on the laser output was also studied in Ref. [11]. Barbieri *et al.*[12] detected the emitted pulse train by a coherent sampling technique and active frequency stabilization. They demonstrated that active mode-locking of THz QCLs can be achieved by modulating the bias current with an RF synthesizer. Freeman *et al.*[12] investigated the dependence of THz pulse width on the modulation power and driven current using an optical sampling technique. Besides, the use of active mode-locking to generate THz frequency combs from QCLs has become a routine affair.[13–15] Forrer *et al.*[16] demonstrated QCL can be injection locked at the cavity roundtrip frequency with small RF powers when devices operated spontaneously in a dense mode regime of harmonic comb state.

Since active mode-locking has been achieved experimentally, while the physical mechanism of short pulse generation from modulated THz QCL with SHB is still poorly understood. The temporal output of lasers with modulation is unknown. In this paper, we simulate active mode-locking dynamics by extensive numerical simulations with and without SHB. First, the impact of the dephasing time on pulse shape is studied. Then the role of modulation parameters on output intensity and duration is clarified. SHB in pulse shaping, stability of mode-locking is discussed. It leads to pulse broadening and destabilization from the laser.

*Project supported by the National Key Research and Development Program of China (Grant No. 2017YFF0106302), the National Natural Science Foundation of China (Grant Nos. 61975225 and 61927813), and Shanghai International Cooperation Project, China (Grant No. 18590780100).

†Corresponding author. E-mail: cwang@mail.sim.ac.cn

‡Corresponding author. E-mail: jccao@mail.sim.ac.cn

© 2020 Chinese Physical Society and IOP Publishing Ltd

2. Theoretical model and main equations

We consider the mode-locking dynamics in THz QCL, which has been studied in Refs. [17,18]. The device was fabricated and processed in 1-mm long and 100-μm wide. The working temperature is 25 K and the threshold is 12.5 kV/cm. The electrons in upper subband 4 arrive at lower subbands by vertical radiation and non-radiative transition, and then experience fast electron-longitudinal phonon scattering relax to subband 1. Finally, the electrons in injector subband 1 are injected into subband 4 of next period. The process then repeats in this period. The dynamics of four subbands system are described by solving one-dimensional full Maxwell–Bloch equations

$$\partial_t n_4 = J - \mathrm{i}\frac{\mathrm{d}E}{\hbar}(P_{43}-P_{43}^*) - \frac{n_4}{t_{43}} - \frac{n_4}{t_{42}} + D\frac{\partial^2 n_4}{\partial z^2}, \quad (1)$$

$$\partial_t n_3 = \mathrm{i}\frac{\mathrm{d}E}{\hbar}(P_{43}-P_{43}^*) + \frac{n_4}{t_{43}} - \frac{n_3}{t_{32}} - \frac{n_3}{t_{31}} + D\frac{\partial^2 n_3}{\partial z^2}, \quad (2)$$

$$\partial_t n_2 = \frac{n_4}{t_{42}} + \frac{n_3}{t_{32}} - \frac{n_2}{t_{21}} + D\frac{\partial^2 n_2}{\partial z^2}, \quad (3)$$

$$\partial_t n_1 = \frac{n_3}{t_{31}} + \frac{n_2}{t_{21}} - J + D\frac{\partial^2 n_1}{\partial z^2}, \quad (4)$$

$$\partial_t P_{43} = -\mathrm{i}\omega P_{43} - \mathrm{i}\frac{\mathrm{d}E}{\hbar}(n_4-n_3) - \frac{P_{43}}{T_2}, \quad (5)$$

$$\partial_z^2 E - \frac{n^2}{c^2}\partial_t^2 E = \frac{Nd}{\varepsilon_0 c^2}\partial_t^2(P_{43}+P_{43}^*). \quad (6)$$

Here, n_4, n_3, n_2, n_1 are the mean occupation probabilities of the corresponding subbands, P_{43} is the off-diagonal element of the density matrix, ω and d are resonant frequency and electric dipole matrix element between subband 4 and subband 3, respectively. T_2 is the dephasing time, which is related to many factors, such as the growth of materials, impurities, and so on. The typical tunneling pure dephasing time ranges from 0.37 ps to 0.44 ps in this device.[19] J is the pumping rate that is proportional to the injection field. As discussed in Refs. [10,12], D is the diffusion coefficient, which is set as zero. n is the refractive index and N is the electron doping concentration. $\mathcal{E}_0$ is the vacuum dielectric constant. We divide the cavity into two sections like mid-infrared QCLs, sinusoidal modulation of the pump current with the roundtrip frequency injected into modulated section and DC current injected into whole cavity, as shown in Fig. 1.

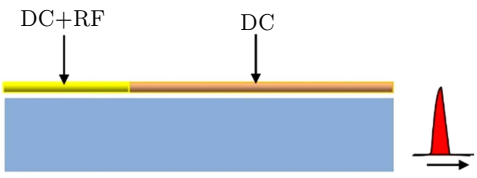


Fig. 1. Active mode-locking is realized by gain modulation with RF signal in THz QCL.

The electric fields propagate in two directions in cavity, and coupled to share the same medium, which gives rise to SHB. The quantities $+$, $-$ represent waves traveling to the right and left directions, respectively. We substitute the ansatz used in Refs. [9–11,20] for Eqs. (1)–(6). In the slowly varying envelope approximation, the equations are transformed to

$$\partial_t n_{40} = J_0 - \frac{n_{40}}{t_{43}} - \frac{n_{40}}{t_{42}} - \mathrm{i}\frac{d}{2h}(E_+\eta_+^* + E_-\eta_-^* - \mathrm{c.c}), \quad (7)$$

$$\partial_t n_{42} = J_2 - \frac{n_{42}}{t_{43}} - \frac{n_{42}}{t_{42}} - \mathrm{i}\frac{d}{2h}(E_+\eta_-^* + E_-^*\eta_+), \quad (8)$$

$$\partial_t n_{30} = \frac{n_{40}}{t_{43}} - \frac{n_{30}}{t_{32}} - \frac{n_{30}}{t_{31}} + \mathrm{i}\frac{d}{2h}(E_+\eta_+^* + E_-\eta_-^* - \mathrm{c.c}), \quad (9)$$

$$\partial_t n_{32} = \frac{n_{42}}{t_{43}} - \frac{n_{32}}{t_{32}} - \frac{n_{32}}{t_{31}} + \mathrm{i}\frac{d}{2h}(E_+\eta_-^* + E_-^*\eta_+), \quad (10)$$

$$\partial_t n_{20} = \frac{n_{40}}{t_{42}} + \frac{n_{30}}{t_{32}} - \frac{n_{20}}{t_{21}}, \quad (11)$$

$$\partial_t n_{22} = \frac{n_{42}}{t_{42}} + \frac{n_{32}}{t_{32}} - \frac{n_{22}}{t_{21}}, \quad (12)$$

$$\partial_t n_{10} = \frac{n_{30}}{t_{31}} + \frac{n_{20}}{t_{21}} - J_0, \quad (13)$$

$$\partial_t n_{12} = \frac{n_{32}}{t_{31}} + \frac{n_{22}}{t_{21}} - J_2, \quad (14)$$

$$\partial_t \eta_+ = \mathrm{i}\frac{d}{2h}[(n_{40}-n_{30})E_+ + (n_{42}-n_{32})E_-] - \frac{\eta_+}{T_2} + \frac{\beta n_{40}}{T_{\mathrm{rad}}}, \quad (15)$$

$$\partial_t \eta_- = \mathrm{i}\frac{d}{2h}[(n_{40}-n_{30})E_- + (n_{42}^*-n_{32}^*)E_+] - \frac{\eta_-}{T_2} + \frac{\beta n_{40}}{T_{\mathrm{rad}}}, \quad (16)$$

$$\left(\frac{n}{c}\partial_t + \partial_z\right)E_+ = \mathrm{i}\frac{\mathrm{d}\omega N}{n\varepsilon_0 c}\eta_+ - l_w E_+, \quad (17)$$

$$\left(\frac{n}{c}\partial_t - \partial_z\right)E_- = \mathrm{i}\frac{\mathrm{d}\omega N}{n\varepsilon_0 c}\eta_- - l_w E_-. \quad (18)$$

Here, l_{w} is the waveguide loss. T_{rad} is the spontaneous radiative lifetime and β is the small geometric factor measuring the fraction of spontaneous emission coupled to the transverse laser mode.[11] $E_\pm$ and $\eta_\pm$ are slowing varying envelopes of the electric field and polarization, respectively. $k = n\omega/c$. The electric field E and polarization P_{43} are obtained by multiplying $\mathrm{e}^{-\mathrm{i}(\omega t \mp kz)}$ and $E_\pm$, $\eta_\pm$. The population of subband i is described by $n_i = n_{i0} + n_{i2}\mathrm{e}^{2\mathrm{i}kz} + n_{i2}^*\mathrm{e}^{-2\mathrm{i}kz}$. The injection J has the same form like electron population

$$J = J_0 + J_2\mathrm{e}^{2\mathrm{i}kz} + J_2^*\mathrm{e}^{-2\mathrm{i}kz}. \quad (19)$$

In QCLs, there are also losses upon two cleaved facets caused by reflection, which located at $z = 0$ and $z = L$. At each facet, the reflection law is dictated by the Fresnel laws.

3. Simulation results and discussion

We simulate active mode-locking dynamics without and then with SHB. The parameters used in caculation are listed in Table 1. The modulated section length is expressed by l_{mod}. The DC bias V_{dc} is applied to the whole cavity, and the RF signal on modulated section is written as

$$V_{\mathrm{mod}} = V_{\mathrm{dc}} + V_{\mathrm{mod,amp}}\sin(2\pi t/T_{\mathrm{round}}). \quad (20)$$

Table 1. Parameters used in simulations.

Quantity	Symbol	Value
Dephasing time/ps	T_2	10.0
Life time/ps	t_{43}	31.7
Life time/ps	t_{42}	33.5
Life time/ps	t_{32}	13.5
Life time/ps	t_{31}	2.90
Life time/ps	t_{21}	0.98
Cavity loss/cm^{-1}	$l_{\rm w}$	10.0
Roundtrip time/ps	$T_{\rm round}$	24.0
Refractive index	n	3.60
Electric dipole matrix element/Å	d	57.6e

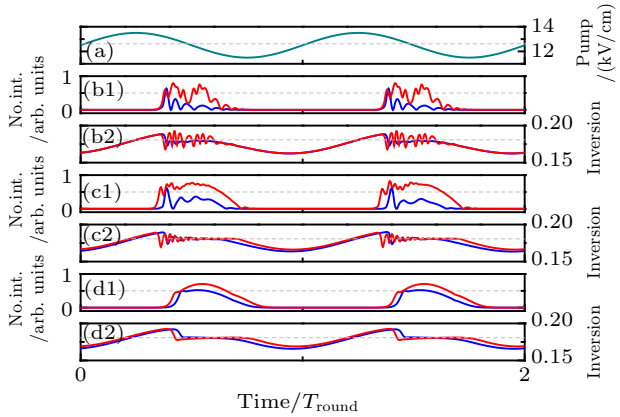


Fig. 2. Pump (a), normalized intensity [(b1), (c1), and (d1)] and inversion [(b2), (c2), (d2)] for middle point inside modulation section for different dephasing times with (red line) and without (blue line) SHB. (b) $T_2 = 10.0$ ps, (c) $T_2 = 1.0$ ps, (d) $T_2 = 0.1$ ps. The abbreviations are listed below. The shorthand notation "Inv." is inversion, "No. int." is normalized intensity.

The dynamics of the THz QCL is investigated when SHB is not included by solving the Maxwell–Bloch equations with $n_{i2} = 0$. To include the SHB in the model we use Eqs. (7)–(18) in the simulation. The DC bias, modulation amplitude and length are fixed at 12.501 kV/cm, 1.0 kV/cm, and 0.008 mm, respectively. The effect of dephasing time in population inversion and resonant tunneling of this device have been discussed in Refs. [18,21]. We still range the dephasing time from 10 ps to 0.1 ps. Figure 2 shows pumping, the evolution of electric field, and the population inversion for middle point inside the modulated section. The effect of dephasing time is much obvious as illustrated in Figs. 2(b)–2(d). Here, the pulse intensity increases and the multiple pulse appears when the dephasing time is increased. For short dephasing time (< 0.1 ps), the envelope of electric field tends to be the single pulse envelope. Since the roundtrip time is close to the gain recovery time, the inversion does not keep in step with the pumping. The inversion is delayed about 0.5π compared with pumping. The pulse peak does not follow the inversion peak due to the long gain recovery time compared to the pulse duration time. The effect of SHB described by the pulse shape is significant. Rapid oscillations within the multiple pulse envelope are generated, both pulse intensity and duration time increase in the presence of SHB. In Fig. 3, we compare the spectral intensity. In the presence of SHB, the number of excited modes is decreased. Also, it will take a long time before the pulse eventually stabilizes.

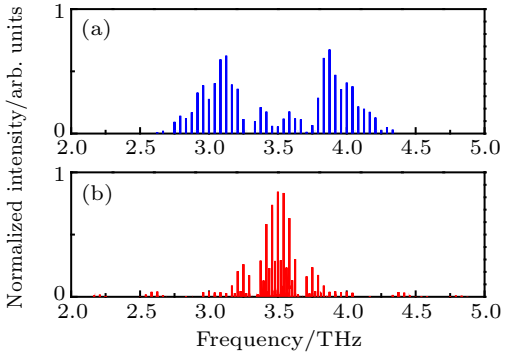


Fig. 3. Spectral intensity for middle point inside modulation section for $T_2 = 10.0$ ps without (a) and with (b) SHB.

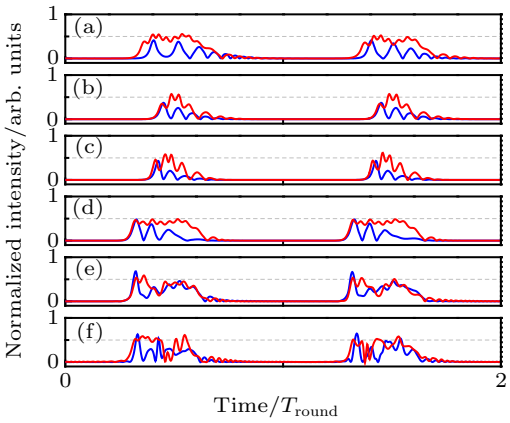


Fig. 4. The output field normalized intensity for different modulation lengths with (red line) and without (blue line) SHB. (a) $l_{\rm mod} = 0.004$ mm, (b) $l_{\rm mod} = 0.008$ mm, (c) $l_{\rm mod} = 0.016$ mm, (d) $l_{\rm mod} = 0.064$ mm, (e) $l_{\rm mod} = 0.128$ mm, (f) $l_{\rm mod} = 0.256$ mm.

Then, the laser dynamics under modulation section length is discussed. Figure 4 shows the intensity of the output pulses for different modulation section lengths and constant modulation pumping. The DC bias and modulation amplitude are fixed at 12.501 kV/cm and 0.4 kV/cm, respectively. As expected, multiple pulse is formed by the effect of long dephasing time. At the same time, the shape of the pulse shows several fine structures due to SHB. The formation of the oscillation is due to the decorrelation of the phase between the modes.[10] The pulse duration time depends on the modulation section length. When the modulated section length $l_{\rm mod}$ increases from 0.004 mm to 0.016 mm, more modes are lasing, the pulse intensity tends to increase and the duration time decrease. For longer modulation length, the window of the net gain becomes wider,[11] resulting the pulse broadening and its intensity rising. Furthermore, the simulated intensity with SHB is greater than that without SHB [Figs. 4(a)–4(d)], which is also clearly seen in Fig. 2. The locked pulse does not exist when $l_{\rm mod}$ increased to 0.256 mm, the pulse duration time almost extends to the whole roundtrip time and its peak intensity varies with $l_{\rm mod}$ irregularly (Fig. 4(f)).

To understand the effect of modulation amplitude $V_{\mathrm{mod,amp}}$ on the output pulse, in Fig. 5, we show the output laser field for varying modulation amplitude. The THz QCL has a fixed DC bias of 12.501 kV/cm and modulation length of 0.008 mm. The modulation section acts as a gain modulator, which drives a large number of longitudinal modes above threshold. As the modulation amplitude increases, we find that the output field of the laser is pulsed and the intensity of the pulse increases as the applied $V_{\mathrm{mod,amp}}$ increases. It is interesting to note that when the laser working at 1.005 kV/cm, the oscillations within multiple pulse envelope are stronger than the laser works at 0.3 kV/cm in the presence of SHB.

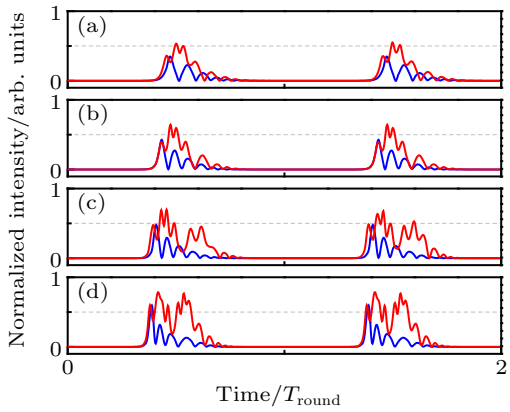


Fig. 5. The output field normalized intensity for different modulation amplitudes with (red line) and without (blue line) SHB. (a) $V_{\mathrm{mod,amp}} = 0.3$ kV/cm, (b) $V_{\mathrm{mod,amp}} = 0.5$ kV/cm, (c) $V_{\mathrm{mod,amp}} = 0.7$ kV/cm, (d) $V_{\mathrm{mod,amp}} = 1.005$ kV/cm.

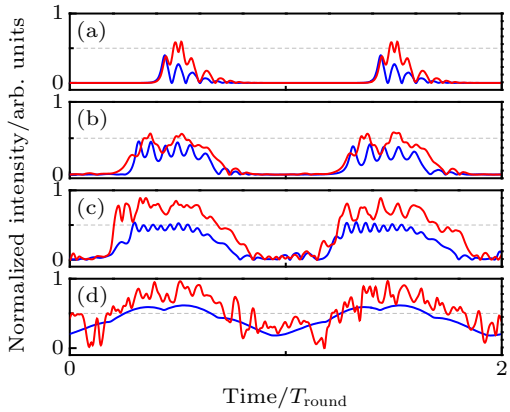


Fig. 6. The output field normalized intensity for different DC bias with (red line) and without (blue line) SHB. (a) $V_{\mathrm{dc}} = 12.501$ kV/cm, (b) $V_{\mathrm{dc}} = 12.51$ kV/cm, (c) $V_{\mathrm{dc}} = 12.55$ kV/cm, (d) $V_{\mathrm{dc}} = 12.6$ kV/cm.

In Fig. 6, we simulate the output intensity for various DC bias when modulation amplitude and length are fixed at 0.45 kV/cm and 0.008 mm. The unmodulated section works as an amplifier, which will lead the pulse reshaping towards longer duration. When the DC bias is close to threshold, the pulse is weak. The amplifier is weakly saturated, which minimizes the pulse lengthening. With increasing of DC bias, the output intensity increases and the gain saturation broadens the pulse clearly. As explained above, the pulse intensity and duration time increase as the DC bias increases. There is no isolated pulse when DC bias is greater than 12.55 kV/cm, and only the intensity is modulated, as shown in Figs. 6(c)–6(d). The output electric field turns into chaotic pulsations in the presence of SHB as shown in Fig. 6(d).

4. Conclusion

We have numerically studied the active mode-locking dynamics of THz QCLs with Maxwell–Bloch equations. It is found that the pulse performance of QCL with a long dephasing time is much more complex as compared to that with a short dephasing time. The output pulse intensity varies with modulation length and pumping. A stable short pulse is generated when DC bias approaches the threshold bias. Besides, the pulse duration time can be controlled by tuning the modulation length at a suitable position. SHB helps to increase the output intensity and duration, but deteriorates the pulse quality and makes the pulse oscillating.

References

[1] Faist J, Capasso F, Sivco D L, Sirtori C, Hutchinson A L and Cho A Y 2002 *Science* **264** 5158
[2] Freeman R J, Maysonnave J, Jukam N, Cavalie P, Maussang K, Beere H E, Ritchie D A, Mangeney J, Dhillon S S and Tignon J 2012 *Appl. Phys. Lett.* **101** 181115
[3] Zewail A H 2000 *J. Phys. Chem. A* **104** 24
[4] Debarre D, Supatto W, Pena A M, Fabre A, Tordjmann T, Combettes L, Schanne-Klein M C and Beaurepaire E 2006 *Nat. Methods* **3** 47
[5] Lee A W M, Williams B S, Kumar S, Hu Q and Reno J L 2006 *IEEE Photon. Technol. Lett.* **18** 1415
[6] Scalari G, Walther C, Faist J, Beere H and Ritchie D 2006 *Appl. Phys. Lett.* **88** 141102
[7] Mottaghhizadeh A, Gacemi D, Laffaille P, Li H, Amanti M, Sirtori C, Saantarelli G, Hansel W, Holzwart R, Li L H, Linfield E H and Baebieri S 2017 *Opt. Lett.* **4** 168
[8] Paiella R, Capasso F, Gmachl C, Hwang H Y, Sivco D L, Hutchinson A L, Cho A Y and Liu H C 2000 *Appl. Phys. Lett.* **77** 169
[9] Wang C Y, Kuznetsova L, Gkortsas V M, Diehl L, Kartner F X, Belkin M A, Belyanin A, Li X, Ham D, Schneider H, Grant P, Song C Y, Haffouz S, Wasilewski Z R, Liu H C and Capasso F 2009 *Opt. Express* **17** 12929
[10] Gkortsas V M, Wang C, Kuznetsova L, Diehl L, Gordon A, Jirauschek C, Belkin M A, Belyanin A, Capasso F and Kartner F X 2010 *Opt. Express* **18** 1316
[11] Wanng Y R and Belyanin A 2015 *Opt. Express* **23** 4173
[12] Barbieri S, Ravaro M, Gellie P, Santarelli G, Manquest C, Sirtori C, Khanna S P, Linfield E H and Davies A G 2011 *Nat. Photon.* **5** 306
[13] Wang F, Pistore V, Riesch M, Nonng H, Vigeron P B, Colombelli R, Parillaud O, Mangeney J, Tignon J, Jirauschek C and Dhillon S S 2020 *Light Sci. Appl.* **9** 51
[14] Bachmann D, Rösch M, Süess M, Beck M, Unterrainer K, Darmo J, Faist J and Scalari G 2016 *Optica* **3** 1087
[15] Piccardo M, Kazakov D, Rubin N A, Chevalier P, Wang Y R, Xie F, Lascola K, Belyanin A and Capasso F 2018 *Optica* **5** 475
[16] Forrer A, Franckie M, Stark D, Olariu T, Beck M, Faist J and Scalari G 2020 *ACS Photon.* **7** 784
[17] Luo H, Laframboise S R, Wasilewski Z R, Aers G C, Liu H C and Cao J C 2007 *Appl. Phys. Lett.* **90** 041112
[18] Wang F, Guo X G and Cao J C 2010 *Phys. Rev. B* **81** 045308
[19] Dupont E, Fathololoumi S and Liu H C 2010 *Phys. Rev. B* **81** 205311
[20] Gordon A, Wang C Y, Diehl L, Kartner F X, Belyanin A, Bour D, Corzine S, Hofler G, Liu H C, Schneider H, Maier T, Troccoli M, Faist J and Capasso F 2008 *Phys. Rev. A* **77** 053804
[21] Wang F, Guo X G and Cao J C 2011 *J. Appl. Phys.* **108** 083714